Inorganic Chemistry
ARTICLE
pubs.acs.org/IC

# Antiferromagnetic Ground State of Quantum Spins in the Synthetic Imanite, $Ca_3Ti_2Si_3O_{12}$: The Lost Child of the Garnet Family

Martin Valldor,*,[†] André Uthe,[‡] and Reinhard Rückamp[†]

[†]II. Physics Department, University of Cologne, Zülpicher strasse 77, D-50937 Cologne, Germany
[‡]Inorganic Chemistry Department, University of Cologne, Greinstrasse 6, D-50939 Cologne, Germany

Supporting Information

**ABSTRACT:** Large single crystals of the garnet imanite, $Ca_3Ti_2Si_3O_{12}$, were synthesized by a floating zone technique. Near-infrared to visible spectroscopy presents an optical gap of 1.65 eV at 4 K, proving the insulating character of this garnet compound. Electron paramagnetic resonance data indicate that the $d^1$ electron of $Ti^{3+}$ exhibits an orbital contribution to the spin moment ($g$ = 1.859(1)). An antiferromagnetic state is observed below $T_N$ = 7 K, confirmed by magnetic susceptibility and specific heat data. X-ray diffraction investigations on powders and single crystals of imanite reveal that the crystal structure agrees well with expectations: the cubic symmetry $Ia\bar{3}d$ describes all obtained single crystal and powder diffraction data.

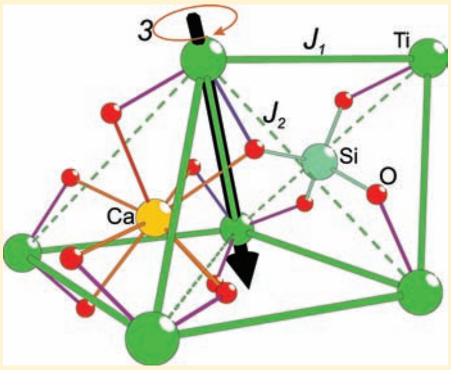

## INTRODUCTION

The garnets[1] constitute one of the largest mineral families and remain an important topic in material sciences and geosciences. A major part of the upper mantle and the high-pressure metamorphic rocks in the crust of our earth incorporates garnets.[2] These gem stones are not only used as jewelry, e.g., $Y_3Al_5O_{12}$ (YAG)[1,3] but also in synthetic form, used as relatively cheap permanent magnets ($Y_3Fe_5O_{12}$, YIG)[4,5] and host matrix for rare-earth ions in laser materials ($Nd^{3+}$:YAG).[6]

Although the chemical flexibility of the garnet structure has been thoroughly investigated, there remains one composition that is less investigated. In an early report on new crystals in titaniferrous slags, the existence of $Ca_3Ti_2Si_3O_{12}$ was mentioned but without further investigations on its properties.[7] This compound was named imanite, a name that was adapted in later works.[8] During investigations of the $CaO-Ti_2O_3-SiO_2$ phase diagram, the imanite was found to be the only a quaternary compound[9] and its garnet type structure was confirmed from an indexed powder pattern. Imanite has not been mentioned since then although $Ti^{3+}$ is a quantum spin ion ($d^1$, $S = {}^1/_2$), which is an interesting species for spectroscopic and magnetic investigations.

Depending on where the magnetic ions are situated in the garnet structure, a variety of magnetic properties can be observed. With the general formula $A_3B_2C_3O_{12}$, it is possible to tentatively divide the garnets into magnetic groups. To limit the discussion in this paper, only a narrow compositional freedom will be considered: 3d transition metals in combination with the nonmagnetic ions $Y^{3+}$, $Ca^{2+}$, $Al^{3+}$, $Si^{4+}$, and $Ge^{4+}$. The $A$ site alone can be described as a three-dimensional net of corner-sharing triangles, as in, spessartine $Mn_3Al_2Si_3O_{12}$ and almandine $Fe_3Al_2Si_3O_{12}$.[10] As a result, strong geometric frustration is expected for magnetic systems with antiferromagnetically coupled spins at the $A$-site, as observed for spessartine.[11] More complex are the magnetic properties for the cases where two of the sites are occupied by magnetic ions. The most well-known example is YIG, having Y at the $A$ site and Fe at the $B$ and $C$ sites. The oxygen coordination of $Fe^{3+}$ is six at $B$ and four at $C$. The magnetic moments at the $B$ and $C$ sites are aligned antiparallel, resulting in a ferrimagnetic ground state.[12] All the known compositions where only $B$ sites contain magnetic ions are antiferromagnets with relatively low transition temperatures. The long superexchange path between the $B$ ions is the reason for the weak spin−spin coupling. For example, andradite, $Ca_3Fe_2Si_3O_{12}$, exhibits a Néel state below 11.5(1) K,[13] and uvarovite, $Ca_3Cr_2Si_3O_{12}$, becomes an antiferromagnet below $T_N$ = 9 K.[14]

In this paper a detailed crystal structure analysis of imanite is presented together with macroscopic measurements concerning its magnetic, thermodynamic, and optic properties.

## EXPERIMENTAL SECTION

**Synthesis.** The precursor $CaSiO_3$ was synthesized through a normal solid state reaction: $CaCO_3$ (99.9%, Merck) was mixed in an agate mortar with $SiO_2$ (99.5%, Alfa-Aesar) in molar ratio 1:1 before the mixture was placed in a corundum crucible and subsequently heated at 1100 °C overnight in air. After the sintered powder was reground, the same heating procedure was repeated. The resulting $CaSiO_3$ was homogenized with

**Received:** May 19, 2011
**Published:** September 12, 2011

$Ti_2O_3$ (99.8%, Alfa-Aesar) and Ti metal (99.99%, Alfa-Aesar) in the relative composition 3.0:0.99:0.02, and the mixture was pressed into a feeding rod (7 cm) and a seed (2 cm). These were subsequently used without prereaction. The single crystal growth was accomplished inside a floating zone mirror image furnace (FZ-T-10000-H-VI-VP). Ar (99.996%) was chosen as reaction gas, and a slight overpressure (0.5 bar) was applied before sealing the reaction chamber; i.e., the crystal growth was performed without continuous gas flow. The turning rates of the feeding rod (∅ ≈ 10 mm) and seed (∅ ≈ 10 mm) were the same, about 10−15 rounds per minute, but in opposite directions. About 90% of full light effect from four 300 W lamps were focused to create the heating zone. High crystallinity was obtained with growth rates in the range 2.5−3 mm/h.

**X-ray Diffraction.** Powder diffraction data were obtained with a standard STOE D5000 diffractometer in reflection (Bragg−Brentano) mode with a Cr X-ray tube ($K\alpha_{1,2}$ $\lambda$ = 2.289 685 and 2.293 586 Å) as photon source. The X-rays were detected with a position sensitive detector (PSD). The diffraction data were evaluated through a Rietveld refinement, using the Fullprof2k software.[15] The Laue images were taken with a standard camera using the whole spectrum of a tungsten X-ray source with 20 keV maximum energy. The detector was an image plate that was read with a BAS-Reader from Fuji. As for the single crystal X-ray experiment, a Bruker Apex2 instrument was used. An empirical absorption correction was applied on the diffraction data using STOE software (X-RED and X-SHAPE).[16,17] The model-to-data comparison including Fourier map calculations was completed with the JANA2000 program.[18]

**Electron Microscopy.** Elemental analyses were performed in a scanning electron microscope SEM515 (Philips) equipped with an EDAX unit at 20 kV acceleration voltage.

**Spectroscopic Measurements.** A single crystal of the title compound was installed on a Bruker ER218G1 goniometer, and angle-dependent electron paramagnetic resonance (EPR) spectra were recorded on a Bruker ELEXSYS 500 equipped with a Bruker ER4141VT temperature controller in the X-band at 9.4 GHz and 100 K using liquid nitrogen as a coolant. Crystalline 2,2-diphenyl-1-picrylhydrazyl (dpph with a *g*-value of 2.0036)[19,20] was used as reference material.

Infrared spectra were obtained with a Bruker FTIR-IFS66v. A halogen light source for the near-infrared and visible range was used together with a $CaF_2$ beam splitter, and the optical windows were made of KBr. The photons were detected with a HgCdTe (MCT) detector and a Si diode. The sample was a single crystal plate that was polished on both sides down to a thickness of about 130 $\mu$m. The cooling was achieved in a continuous flow cryostat with liquid He as cooling agent. In the region of high transmittance, the data exhibited strong Fabry−Pérot fringes. In the data presented here, these fringes were smoothened out for clarity.

**Macroscopic Measurements.** Specific heat data were extracted with a physical properties measurement system (Quantum Design, PPMS) using the nonadiabatic thermal relaxation method in the temperature range from 1.8 to 300 K. The heat pulse for each measurement was 2% of the absolute temperature. Apiezon N grease was used to attach the sample to the previously cleaned sample holder. Before performing the sample measurements, the heat capacity of the grease alone was measured at 200 K, which gives the whole temperature-dependent addenda by scaling its heat capacity on top of that of the cleaned sample holder. This addenda was subtracted from the measured total heat capacity obtained with the single crystalline sample slice (22.75 mg). Magnetic investigations were done in a SQUID MPMS XL7 (Quantum Design) for fields up to 7 T in the temperature range 2−300 K. The single crystal sample was held in place with a thin tape strip. Diamagnetic corrections were not applied on the data because of a relatively strong signal from the sample.

## ■ RESULTS AND DISCUSSIONS

**Basic Properties.** The single crystalline rod appeared dark, almost black (upper inset in Figure 1), but thinner slices revealed that the crystal was transparent and dark red. According to 10 elemental analyses on a crystal slice surface, the metal to metal ratio was Ca2.8(1)/Ti2.2(1)/Si3.0(1). The minor deviations in the Ca and Ti contents are most probably due to the fact that Ti-metal is used for calibrating the analyzing system and its absorption coefficient is higher than for Ti in oxides.

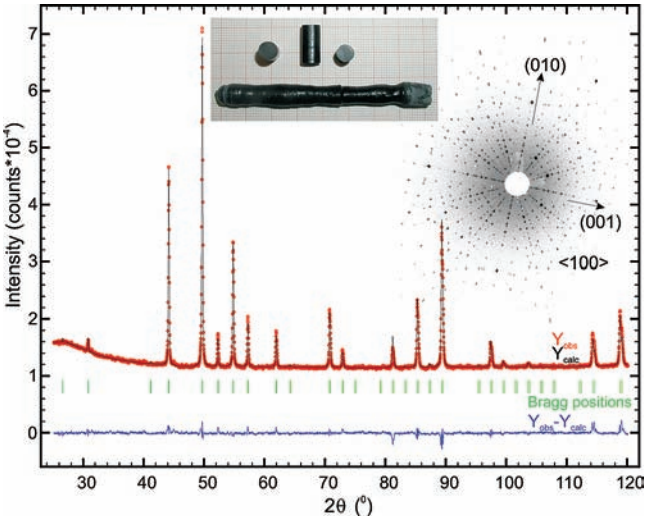

**Figure 1.** Powder X-ray diffraction data of $Ca_3Ti_2Si_3O_{12}$. The observed intensities are marked with open circles, and the Rietveld model is presented with a superposed full black line. The expected Bragg positions are indicated with vertical lines, below which the difference between observed and calculated data is shown. The upper inset is a photo of the single crystalline rods on a millimeter scale paper. Upper right inset displays a Laue image approximately along the *a*-axis.

In the synthesis, Ti metal prevented the appearance of titanate $(CaTiSiO_5)^{21}$ that formed already at very low oxygen pressure. Colorless, transparent titanate crystal impurities, found in rods without Ti metal in the starting mixture, were identified by means of single crystal diffraction.

**Structural Investigation.** The X-ray powder diffraction data from a ground single crystal reveal that the crystal is free from impurities within the limits of detection; i.e., all observed intensities could be indexed and well modeled with a cubic garnet structure (Figure 1). The subsequent Rietveld refinement of the powder data gave the unit cell parameter *a* = 12.1875(2) Å, which was adapted for the single crystalline sample. The fractional coordinates and the thermal displacements of the atoms are not presented here as more accurate values were obtained from the single crystal refinement. As expected, the unit cell parameter *a* is proportional to the *B*-ion size in the series $Ca_3B_2Si_3O_{12}$, and the title compound can be placed in-between $B = Sc^{3+}$ (*a* = 12.22 Å) and $B = V^{3+}$ (*a* = 12.011(1) Å).[10]

Laue images of the melt grown rod reveal that the sample has high crystallinity and is, as suggested from all photos made, a single-domain single crystal. A typical Laue image from $Ca_3Ti_2Si_3O_{12}$ is shown in the upper right inset in Figure 1.

During the single crystal diffraction measurement, a total of 27 919 reflections were measured, of which 1631 were unique with an internal *R*-value of 0.0211. By applying the centered cubic symmetry and the empirical absorption correction, the $R_{int}$ increased to 0.0396, which is a relatively low value considering the large number of symmetry equivalent intensities. After merging the symmetry equivalent reflections, including Friedel

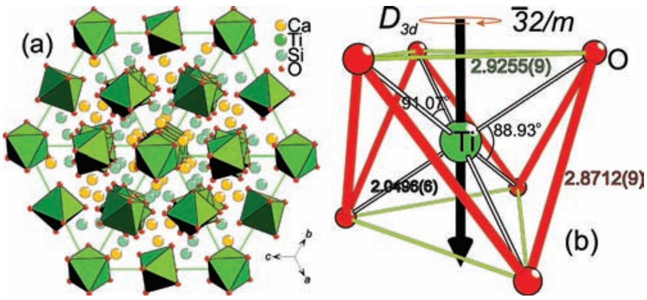

**Figure 2.** (a) Perspective view of the $Ca_3Ti_2Si_3O_{12}$ garnet crystal structure close to the space diagonal of the cubic unit cell (indicated with full lines). The $TiO_6$-polyhedra are marked to highlight how isolated these octahedra are. (b) The trigonally distorted octahedral environment of $Ti^{3+}$. Relevant interatomic distances and angles are presented in angstroms and degrees, respectively. The bonds represented with equal design have the same length. The rotation inversion axis is marked with a thick arrow and the Schönflies as well as the Hermann−Mauguin point group symmetries for $Ti^{3+}$ are added as notations.

pairs, 759 reflections remained, of which 424 had an intensity larger than $3\sigma$ (99.87% significance). The refinement was completed on squared structure factors (intensities), and the initial atomic coordinates were taken from a previously known garnet compound.[3] All parameters not restricted by symmetry were refined: $x$, $y$, $z$ for O, harmonic displacements for all four atom positions, and a scaling parameter, giving a total of mere 17 parameters, as all sites were assumed to be fully occupied. The data/parameters ratio ($\approx$25) is thus acceptable, and the results from the refinement are presented in Supporting Information. In the difference Fourier map, after the final refinement, the largest peak (0.48 $e^-/Å^3$) and hole (−0.51 $e^-/Å^3$) are both close to the resolution limit and, hence, considered insignificant.

**Structure Description.** The garnet crystal structure is shown in Figure 2a, and a detailed structure description can be found elsewhere.[1] The features most important for the discussion on the properties presented in this paper are the following: the oxygen coordinations for the metal ions $Ca^{2+}$, $Si^{4+}$, and $Ti^{3+}$ are 8, 4, and 6, respectively. The coordination environment of the magnetic $Ti^{3+}$ (Figure 2b) can be described as trigonally distorted octahedron, where all Ti−O distances are identical (2.0496(6) Å), but there are two different O−Ti−O angles. All distorted $TiO_6$ octahedra are separated by nonmagnetic $Ca^{2+}$ or $Si^{4+}$, and the shortest Ti−Ti distance is 5.28 Å, i.e., the Ti ions do not share oxygen ions.

From the Ti−O bond length, the bond valence sum can be calculated according to Brown and Altermatt[22] and the formal oxidation state is +3.18. Hence, the mean metal-to-oxygen distance is smaller than the value expected for a $Ti^{3+}$ ion in this coordination. Accordingly, the ligand field splitting of the orbital energy levels is larger than in the case where the formal oxidation state is +3.

**Spectroscopy on $Ti^{3+}$.** The EPR spectrum of a $Ca_3Ti_2Si_3O_{12}$ single crystal at 100 K exhibits a broad isotropic signal, which is indicative of the existence of $Ti^{3+}$ centers (Figure 3). The single crystal was investigated with the applied field along the cubic $a$ axis [100]; on rotating the crystal, setting the $H$-field along [110], the signal did not change (data not shown). The single unpaired electron of the $d^1$ configuration gives rise to the signal generally, whereas the isotropic shape and independence on the angle is due to the high symmetry of the crystalline compound.

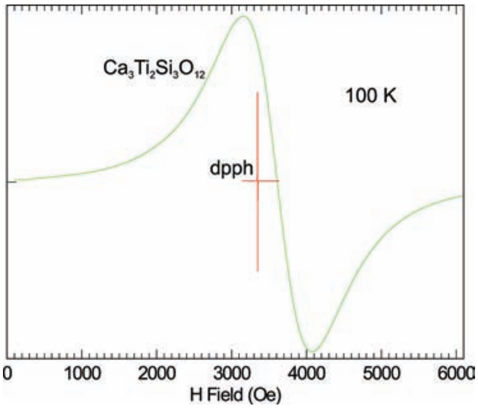

**Figure 3.** EPR spectrum of $Ca_3Ti_2Si_3O_{12}$ and dpph at 100 K as function of magnetic field.

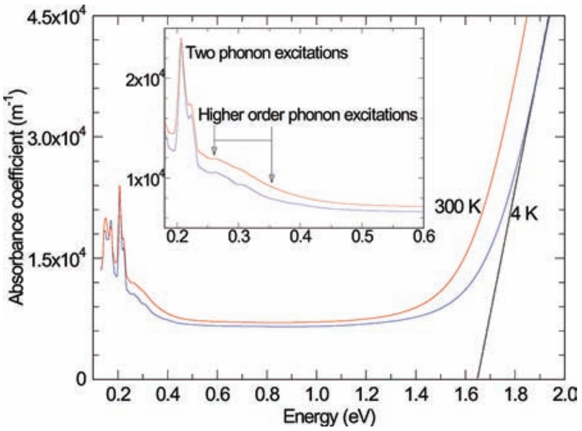

**Figure 4.** Absorbance coefficients of single crystalline $Ca_3Ti_2Si_3O_{12}$ at two different temperatures as functions of photon energy. The dashed line represents the extrapolation of the 4 K curve. The inset is a magnification of the low energy range with two marked phonon ranges discussed in the text.

The Landé factor of the sample $g_{iso}$ = 1.859(1) is smaller than the theoretical spin-only value of 2. For a less than half filled d-shell $S$ is expected to be antiparallel to $L$ and a $g$-factor lower than 2 indicates a contribution of an orbital angular momentum ($L$). Its value can be calculated by combining the relations $J = S - L$ and $g = 1 + ((S(S+1) + J(J+1) - L(L+1))/(2J(J+1)))$. Assuming that $S = {}^1/_2$ and inserting the measured $g$-factor, an $|L| \approx 0.0844$ is obtained, which is a reasonable average for the quantum spins. In our experiment, no hyperfine-splitting between the unpaired electrons and the Ti nuclei, namely the two EPR active isotopes $I(^{47}Ti) = {}^5/_2$, $I(^{49}Ti) = {}^7/_2$, is observed. Instead there is a broad signal with a width of 930 G, which is common for transition metals and therefore expected for Ti as well. Two reasons account for the line broadening: the dipole−dipole interactions between paramagnetic centers and the electronic exchange interaction via orbital overlap.

The optical data of single crystalline imanite, shown in Figure 4, is typical for an insulating sample. At low energies the transmittance is limited by the onset of the phonon absorptions. The weak absorptions, shown in the inset in Figure 4, are assigned to multiphonon excitations; the peaks between 0.20 and 0.23 eV represent the two phonon continuum containing

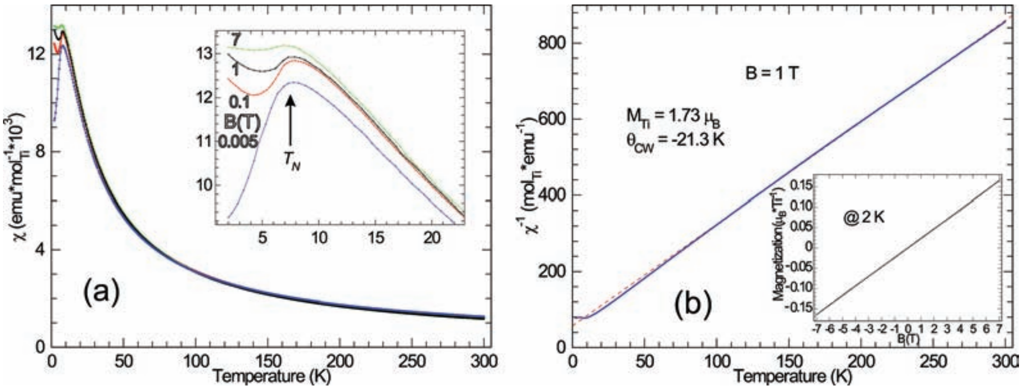

**Figure 5.** (a) Magnetic susceptibilities ($\chi$) of $Ca_3Ti_2Si_3O_{12}$ as functions of temperature in four different applied fields, as indicated in the inset. (b) Inverse $\chi$ in a 1 T field, where a Curie−Weiss fit is marked with a dashed line. The inset displays the field dependent magnetization at 2 K. In all measurements, the *B*-field was applied along the crystallographic *a*-axis.

two prominent maxima. Note that the difference of these excitations between room- and base-temperature is unusually small. The observed anomalies in the range 0.27−0.33 eV get more pronounced at low temperatures: this is a typical scenario for phonon excitations, but their energies indicate that the excitations involve more that two phonons. Within the gap, none of the d−d transitions of the $Ti^{3+}$ ions were observed, implying that these excitations have higher energies, i.e., are found above the gap, with a high transmittance below the band gap and above the phonon range. A rough estimation of the band gap at 4 K is 1.65 eV, by linear extrapolation from the onset of the electronic excitation (Figure 4). As expected, the band gap decreases with increasing temperature. The d−d transitions are forbidden by parity selection rules, but can occur in the form of weak absorptions, due to a two particle process involving an additionally excited phonon.[23]

Thus, the dark red color, as observed by the naked eye, can be understood in the following way: only the red part of the visible spectrum can pass through the sample, whereas for higher frequencies, the sample is opaque. This property is desired in color filtering applications.

**Magnetism.** The magnetic susceptibility ($\chi$), shown in Figure 5a, exhibits a typical paramagnetic behavior at high temperatures. Using a Curie−Weiss fit to the data in the range 250−300 K, according to $\chi^{-1} = (2.83/(M_{Ti}))^2 \times (T + \theta_{CW})$, a paramagnetic moment for $Ti^{3+}$ ion was estimated to be 1.73 $\mu_B$ (Figure 5b). This would perfectly fit the theoretical magnetic moment for a fully quenched orbital moment ($g = 2$). However, the measured $g$-factor from the EPR spectroscopy indicates that a part of the orbital moment is active, suppressing the spin moment. Using the calculated orbital moment, the relation $\mu_{L+S} = ((4S(S+1)) + (L(L+1)))^2$, and the fact that the orbital moment is antiparallel to the spin moment, the expected paramagnetic moment should be 1.705 $\mu_B$, agreeing with the observation.

The negative Weiss constant ($\theta_{CW}$ = −21 K) suggests a preference for an antiparallel spin state in the fluctuating paramagnetic state. $\chi$ decreases below a magnetic anomaly at 7 K, indicating an antiferromagnetic (Néel) ordering of the spin system. By increasing the measuring field, this decrease can be partly canceled, so that $\chi$ levels out below $T_N$ at 7 T, but the anomaly remains at the same temperature (inset Figure 5a). Obviously, the higher fields cant the spins in the ordered state. This is expected, because the magnetic field energy is about a third of the spin−spin coupling, as estimated from the Weiss constant. This also explains the relatively high magnetization reached in field up to 7 T at 2 K (Figure 5b): 0.15 of the possible 1 $\mu_B$, i.e., almost $^1/_6$ of full spin polarization.

It is surprising to observe such relatively strong spin−spin coupling in a spin quantum system ($S = {}^1/_2$) with magnetic entities spatially so far apart. The large number of magnetic nearest neighbors (8 at 5.28 Å) and next nearest (6 at 6.09 Å) neighbors probably play an important role.

Normally, the magnetic coupling strength scales with the size of the spin, if no other parameters are relevant. This also applies for the garnets in the compositional series $Ca_3B_2Si_3O_{12}$: $B = Fe^{3+}$ ($d^5$, $S = {}^5/_2$) $T_N$ = 11.2 K;[13] $B = Cr^{3+}$ ($d^3$, $S = {}^3/_2$) $T_N$ = 9 K;[14] and in the title compound $B = Ti^{3+}$ ($d^1$, $S = {}^1/_2$) $T_N$ = 7 K. Unless further parameters are important, it is possible to estimate Néel temperatures for $B = V^{3+}$ ($d^2$, $S = 1$) and $B = Mn^{3+}$ ($d^4$, $S = 2$) to be $T_N$ = 8 and 10 K, respectively. Unfortunately, no data are available for the last two garnets to confirm this simple trend.

The Néel order formed at approximately 7 K is at a third of the expected value ($T_N(\exp) \approx \theta_{CW}$). Hence, $T_N$ is for some reason suppressed. In antiferromagnets, geometrical effects can cause spin frustration, especially in connection with triangular units. A closer examination of the Ti sublattice (Figure 6) reveals a possible explanation for the relatively low $T_N$. The shortest Ti−Ti distances (5.28 Å) constitute a 3D lattice of distorted squares (thick lines in Figure 6b, $J_1$), which alone cannot induce frustration in an antiferromagnet. However, possible coupling between next nearest Ti−Ti neighbors, on distances of 6.09 Å, is found on the diagonal of each square ($J_2$, dashed line in Figure 6b). This would cause a geometrical frustration if this spin−spin coupling ($J_2$) is antiferromagnetic and comparable to $J_1$ in strength. A competition between $J_1$ and $J_2$ is the most reasonable explanation for the low $T_N$, but it has to be confirmed either through an inelastic neutron scattering experiment or similar.

The magnetic superexchange path has to include either $SiO_4$, $CaO_8$, or both. In Figure 6, the incorporation of these two units in the garnet structure is displayed. It is fair to assume that the relatively covalent $SiO_4$ tetrahedron is more likely to serve as magnetic mediator, due to its strongly correlated electrons in the molecular orbitals. Through *ab initio* all electron calculations, Meyer et al. confirmed that the $SiO_4$ unit is the mediating entity for the magnetic coupling in the cases $Ca_3Cr_2Si_3O_{12}$ and $Ca_3Fe_2Si_3O_{12}$.[24] However, the suggested superexchange paths are via Cr−O−Si−O−Cr in the former and via Fe−O−O−Fe

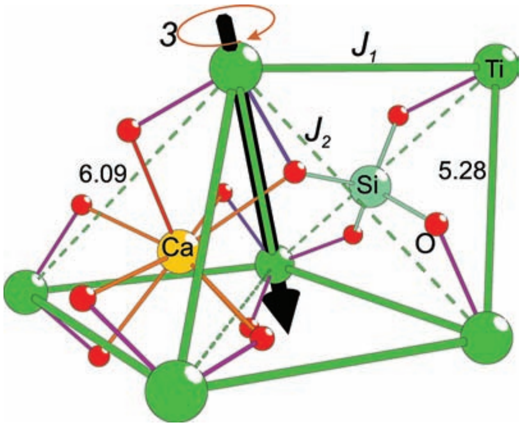

**Figure 6.** Selected part of the $Ca_3Ti_2Si_3O_{12}$ crystal structure. Solid thin lines between ions display possible nearest neighbor superexchange interactions ($J_1$). Dashed lines indicate the next nearest neighbor Ti−Ti interactions ($J_2$). The 3-fold rotational symmetry is marked with an arrow, which is representing the space diagonal of unit cell.

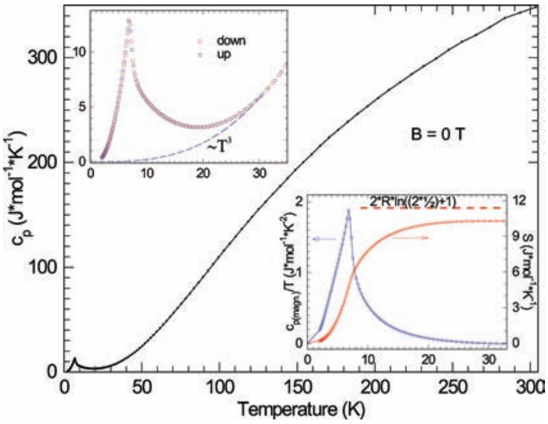

**Figure 7.** Specific heat ($c_p$) of $Ca_3Ti_2Si_3O_{12}$ at zero magnetic field. A line has been drawn between the data points to guide the eye. The upper left inset shows the low temperature region and contains data from a heating (up) and a cooling (down) measurement; the dashed line represents the lattice contribution to $c_p$, i.e., Debye estimation of phonons. The inset (low right) contains the magnetic $c_p/T$ vs $T$ and its integral, entropy $S$, for the lowest temperatures. The theoretical magnetic entropy of a $S = 1/2$ system is drawn with a dashed horizontal line in the lower right inset.

in the latter. Note that Si is supposed to be inactive in the most significant superexchange mechanism in $Ca_3Fe_2Si_3O_{12}$. Those interpretations from the calculations were used to explain the two different antiferromagnetic ground states found experimentally in the closely related germanate garnets. For $Ca_3Ti_2Si_3O_{12}$, a neutron scattering experiment below $T_N$ will reveal the preferred magnetic structure of the quantum spins and perhaps hint at the corresponding superexchange path.

The observed spin frustration from the magnetic susceptibility could perhaps be a consequence of the chosen superexchange path, i.e., via the $SiO_4$ unit. Without further investigations it is difficult to explain the frustration, but it will only be active if $J_2$ is of the order as $J_1$.

**Specific Heat.** To establish the order of the phase transition close to 7 K seen in the magnetic susceptibility, the specific heat was measured in the range of the transition and up to room temperature. The obtained data are shown in Figure 7. Two observations suggest a second order phase transition: (i) the broadness of the anomaly close to 7 K and its asymmetry and (ii) the absence of a detectable hysteresis of the anomaly during heating and cooling cycles (upper left inset in Figure 7). In a simple approximation, the phononic contribution to $c_p$ is proportional to $T^3$ at low temperatures (upper left inset in Figure 7) and can thus be subtracted from the total specific heat, to obtain the magnetic contribution. Unfortunately, the Debye temperature cannot be well estimated due to the significant magnetic contribution at low temperatures, where the Debye $T^3$ approximation is fully valid. To estimate the magnetic entropy, $c_{p(magn)}/T$ is plotted as function of $T$ (lower inset in Figure 7). Here, it is assumed that $c_p/T(T)$ is linear with $T$ in the range 0−2 K and that $c_p/T \rightarrow 0$ as $T \rightarrow 0$; i.e., the ground state has no residual entropy. The integration $\int((C_{p(magn)})/T)\,dT$, i.e., the entropy $S$, saturates close to 10.3 J mol$^{-1}$ K$^{-1}$, which is about 90% of the theoretical value for a $S = {}^1/_2$ system (lower right inset in Figure 7). Considering the approximations made, the calculation suggests a fully ordered spin ground state.

Moreover, the lack of first order phase transitions in the temperature range proves that the room-temperature crystal symmetry is preserved down to 2 K.

The high temperature end of the specific heat data does not apprach the Dulong−Petit limit ($3RN = 3 \times 8.3145 \times 20 = 498.9$ J mol$^{-1}$ K$^{-1}$). However, the room-temperature specific heat of imanite (346 J mol$^{-1}$ K$^{-1}$) agrees well with those of similar garnets: andradite $Ca_3Fe_2Si_3O_{12}$ (352 J mol$^{-1}$ K$^{-1}$),[25] uvarovite $Ca_3Cr_2Si_3O_{12}$ (321 J mol$^{-1}$ K$^{-1}$),[14] and the nonmagnetic grossular $Ca_3Al_2Si_3O_{12}$ (333 J mol$^{-1}$ K$^{-1}$).[26] Thus, there is a systematic discrepancy that depends on the limited measured temperature range; high temperature specific heat measurements on pyrope ($Mg_3Al_2Si_3O_{12}$), grossular,[27] and almandine ($Fe_3Al_2Si_3O_{12}$)[28] reveal that the expected Dulong−Petit limit is reached at temperatures close to 1000 K.

## ■ CONCLUSIONS

By replacing a small part of $Ti_2O_3$ by Ti metal in the starting mixture with $CaSiO_3$, it is possible to synthesize large single crystals of pure imanite by the optical floating zone technique. Minor orbital moments are observed for the quantum spins on $Ti^{3+}$, and a Néel state is observed below a second order phase transition at 7 K. Imanite has an optical gap of 1.65 eV, which points at a typical insulating character. The crystallographic, thermodynamic, and magnetic data are in line with expectations, in comparison with previously reported garnets.

## ■ ASSOCIATED CONTENT

Ⓢ **Supporting Information.** Listings of atomic parameters from single crystal refinement, including $R$-values, GOF values, and harmonic thermal displacement parameters. This material is available free of charge via the Internet at http://pubs.acs.org.

## ■ AUTHOR INFORMATION

### Corresponding Author

*E-mail: valldor@ph2.uni-koeln.de. Fax: 0049-221-470-6708.

## ■ ACKNOWLEDGMENT

We want to thank Inge Simons and Oliver Breunig for performing the EDX analyses and for helping us evaluate the specific heat data, respectively. This work was financed by the German Research Foundation (DFG) through Project SFB608.

## ■ REFERENCES

(1) Menzer, G. *Z. Kristallogr.* **1928**, *69*, 300.

(2) Deer, W.; Howie, R.; Zussman, J. *An Introduction to the Rock Forming Minerals*; Wiley: New York, 1992.

(3) Yoder, H. S.; Keith, M. L. *Geol. Soc. Am. Bull.* **1950**, *61*, 1516.

(4) Bertaut, F.; Forrat, F. *C. R. Acad. Sci. (Paris)* **1956**, *242*, 382.

(5) Geller, S.; Gilleo, M. A. *Acta Crystallogr.* **1957**, *10*, 239.

(6) Geustic, J. E.; Marcos, H. M.; Van Uitert, L. G. *Appl. Phys. Lett.* **1964**, *4*, 182.

(7) Rudneva, A. V. *Akad. Nauk. S.S.S.R., Inst. Khimii Silikatov* **1958**, 285.

(8) Fleischer, M. *Am. Mineral.* **1959**, *44*, 907.

(9) Ye, G. Z.; Rosenqvist, T. *Scand. J. Metall.* **1991**, *20*, 222.

(10) Novak, G. A.; Gibbs, G. V. *Am. Mineral.* **1971**, *56*, 791.

(11) Lau, G. C.; Klimczuk, T.; Ronning, F.; McQueen, T. M.; Cava, R. J. *Phys. Rev. B* **2009**, *80*, 214414.

(12) Rodic, D.; Mitric, M.; Tellgren, R.; Rundlof, H.; Kremenovic, A. *J. Magn. Magn. Mater.* **1991**, *191*, 137.

(13) Murad, E. *Am. Mineral.* **1984**, *69*, 722.

(14) Klemme, S.; van Miltenburg, J. C.; Javorsky, P.; Wastin, F. *Am. Mineral.* **2005**, *90*, 663.

(15) Rodriguez-Carvajal, J. *Physica B* **1993**, *192*, 55.

(16) *X-RED, v. 1.07*; STOE & Cie GmbH: Darmstadt, Germany, 1996.

(17) *X-SHAPE, v. 1.01* ; STOE & Cie GmbH: Darmstadt, Germany, 1996.

(18) Petříček, V.; Dušek, M. *Jana2000*; Institute of Physics AVCR: Praha, Czech Republic, 2002.

(19) Poole, C. P. *Electron Spin Resonance: A Comprehensive Treatise on Experimental Techniques*; Dover Publications: Mineola, NY, 1996.

(20) Davies, M. J. *Electron Paramagnetic Resonance*; Royal Society of Chemistry: Cambridge, U.K., 2000.

(21) Zachariasen, W. H. *Z. Kristallogr.* **1930**, *73*, 7.

(22) Brown, I. D.; Altermatt, D. *Acta Crystallogr., Sect. B* **1985**, *41*, 244.

(23) Rückamp, R.; Benckiser, E.; Haverkort, M. W.; Roth, H.; Lorenz, T.; Freimuth, A.; Jongen, L.; Möller, A.; Meyer, G.; Reutler, P.; Büchner, B.; Revcolevschi, A.; Cheong, S.-W.; Sekar, C.; Krabbes, G.; Grüninger, M. *New J. Phys.* **2005**, *7*, 144.

(24) Meyer, A. A.; Pascale, F.; Zicowich-Wilson, C. M.; Dovesi, R. *Int. J. Quantum Chem.* **2010**, *110*, 338.

(25) Robie, R.; Bin, Z.; Hemingway, B. R.; Barton, M. D. *Geochim. Cosmochim. Acta* **1987**, *51*, 2219.

(26) Haselton, H. T., Jr.; Westrum, E. F., Jr. *Geochim. Cosmochim. Acta* **1980**, *44*, 701.

(27) Hofmeister, A. M.; Chopelas, A. *Am. Mineral.* **1991**, *76*, 880.

(28) Mittal, R.; Chaplot, S. L.; Choudhury, N.; Loong, C.-K. *Phys. Rev. B* **2000**, *61*, 3983.